Available online at www.sciencedirect.com
ScienceDirect
Polymer 48 (2007) 4537–4546
polymer
www.elsevier.com/locate/polymer

# Microphase separation and molecular conformation of $AB_2$ miktoarm star copolymers by dissipative particle dynamics

Ching-I Huang*, Hsu-Tung Yu

*Institute of Polymer Science and Engineering, National Taiwan University, Taipei 106, Taiwan*

Received 21 December 2006; received in revised form 11 May 2007; accepted 1 June 2007
Available online 8 June 2007

**Abstract**

We simulate the microphase separation behavior and analyze the molecular conformation of $AB_2$ miktoarm star copolymers via dissipative particle dynamics (DPD). The phase diagram is constructed by varying the composition and interaction parameter. Through a mapping of the interaction parameter for a finite chain length, we find that the phase diagram via DPD is in near quantitative agreement with that predicted by the self-consistent mean-field (SCMF) theory. However, when the B composition is small, $AB_2$ is not able to form the ordered microstructure as easily as SCMF has predicted. Instead, only a tube-like phase is formed. This aggregated micelle-like phase via DPD, which is ignored in the SCMF study, has been frequently observed in experiments. In the analysis of the radius of gyration ($R_g$), when the interaction parameter increases, the $R_g$ values of each A and B arm remain relatively unchanged; while the overall radius of gyration of $AB_2$ significantly increases. Furthermore, the angle between A and B arms shows an increasing trend while the angle between B and B arms shows a decreasing behavior with the interaction parameter. These results reveal that in order to reduce the contacts between A and B, the A and B arms tend to separate from each other, and the two B arms are squeezed onto the same side.


*Keywords:* Dissipative particle dynamics; Miktoarm star copolymers; Microphase separation

## 1. Introduction

Due to its variant self-assembling behavior, block copolymers are widely applied in many nanotechnologies, such as photonic and biotechnological applications [1,2]. Earlier studies have mainly focused on linear block copolymers [1–4], whose microstructure type is mainly dominated by the value of $\chi N$ ($\chi$ is the Flory–Huggins interaction parameter, $N$ is degree of copolymerization) and the composition $f$. Recently, with the improvement in synthetic techniques, copolymers with more complex architectures, such as star, comb and cyclic, have been successfully synthesized. Their microstructures impose different influences upon various properties of polymers, such as mechanical and photoelectronic properties. Hence, exploring the effects of molecular architecture on the resulting microphase separation of copolymers becomes a vital and interesting topic.

Miktoarm star copolymers, as shown in Fig. 1(a), are one of the molecular architectures that have attracted a lot of attention. Theoretically, Olvera de la Cruz and Sanchez [5] were among the first to examine the stability criteria of microstructures formed by star copolymers. They found that a simple graft $AB_2$ copolymer is more difficult to undergo a microphase separation than a linear AB copolymer due to the greater change of entropy loss associated with the disorder-to-order transition. Milner et al. [6,7] later applied the strong segregation theory (SST) to construct the phase diagram of $A_mB_n$ miktoarm star copolymers in terms of the composition and the asymmetric parameter $\varepsilon$ ($=(n_A/n_B)(l_A/l_B)^{1/2}$), where $n_I$ and $l_I$ are the number of arms and characteristic length of component I, I = A, B, respectively. The length parameter $l_I$ is defined as $l_I = V_I/R_I^2$, where $V_I$ and $R_I$ correspond

* Corresponding author. Tel.: +886 2 33665886; fax: +886 2 33665237.
*E-mail address:* chingih@ntu.edu.tw (C.-I. Huang).

0032-3861/$ - see front matter © 2007 Elsevier Ltd. All rights reserved.
doi:10.1016/j.polymer.2007.06.002

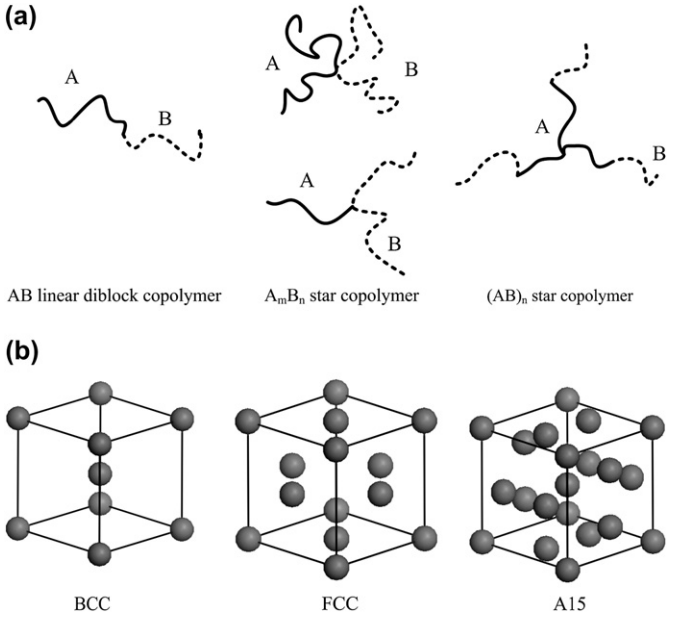


Fig. 1. Schematic representation of (a) miktoarm star diblock copolymers and (b) spherical packing lattices.

to the molecular volume and the radius of gyration of the respective blocks I. They reported that at the same composition, varying the asymmetric parameter $\varepsilon$ could trigger the evolvement of various microstructures. For instance, when the A composition $f_A = 0.5$, increasing the number of B arms in the $AB_n$ miktoarm star copolymers is analogous to decreasing $f_A$, and thereafter a series of transition from lamellae $(L) \rightarrow$ gyroid of minority A $(G_A) \rightarrow$ hexagonally-packed A-formed cylinders $(C_A^{HEX}) \rightarrow$ A-formed spheres $(S_A)$ is expected. This is reasonable since the component with more arms experiences more lateral crowding and becomes more stretched; it tends to remain on the outside domains. Recently, Grason and Kamien [8] employed the self-consistent mean-field (SCMF) theory to construct the phase diagram of $AB_n$ miktoarm star copolymers in terms of $f_A$ and $\chi N$. Comparing with diblock copolymers, the order-disorder transition (ODT) curve raises to larger values of $\chi N$, and the phase diagram is no longer symmetric at about $f_A = 0.5$ and shifts toward $f_A > 0.5$. That is, the stability of microstructures with the B blocks in the majority domains is enhanced as the number of B arms $n$ increases. Moreover, the effects of molecular asymmetry on the shifting degree of the phase diagram reache a limit when $n > 3$. It is worth to mention that other than the regular microstructures formed by linear AB diblock copolymers, such as L, G, $C^{HEX}$, and body-centered cubic arrays of spheres ($S^{BCC}$), they observed a significantly stable regime of A15 packing array of A-formed spheres, as illustrated in Fig. 1(b). Ordinarily, there are two kinds of commonly seen spherical packing orders in linear AB diblock copolymer melts and solutions: BCC and face-centered cubic (FCC). The A15 phase has received quite some attention lately since it has also been proposed as a quite possible state in other complex architectures, such as dendrimer [9] and multi-branch [10] copolymers. Basically, these theoretical results are in good agreement with experimental results, except in the stability of spherical packing order and when the composition of single arm A is larger [11–17]. For example, Pochan et al. [11] used transmission electron microscopy (TEM) and small angle X-ray scattering (SAXS) to examine the phase behavior of polystyrene (PS)–polyisoprene $(PI)_2$ miktoarm star copolymers. They observed similar results as predicted by theory; however, when the composition of PS is relatively high ($f_{PS} = 0.81$), PS–$PI_2$ copolymers are not able to form an ordered $C_A^{HEX}$ phase but only worm-like micelles, and the A15 phase has not been observed yet. Later Tselikas et al. [13] applied TEM and SAXS to examine the $(PS)_m$–$(PI)_n$ miktoarm star copolymers. By varying the asymmetric parameter $\varepsilon$ the observed microstructures fit well with the theoretical results. Lee et al. [14] applied TEM and small angle neutron scattering (SANS) to examine the phase behavior of asymmetric PS–$PI_2$ and PS–$PI_3$ miktoarm star copolymers. In a comparison with the symmetric miktoarm star copolymers, they observed that although there is not much difference in the morphology type but the chain stretching degree on the outside domains is partially reduced by the asymmetric PI arms. Yang et al. [16] examined the PS–$PI_5$ miktoarm star copolymers, and found that as SCMF theory predicted, the corresponding phase diagram did not shift when the asymmetric parameter $\varepsilon$ was high enough to reach a certain value.

Just as previously stated, although the phase diagram regarding $AB_n$ miktoarm star copolymers has been predicted by SCMF theory, unfortunately neither the fluctuation effects nor the hydrodynamic interactions are included. The former plays an important role in determining the ODT curve [18], and the latter has a great influence on the kinetics of microphase separation [19]. Recently, a newly developed dissipative particle dynamics (DPD) simulation method, which considers the hydrodynamic interactions and the fluctuations, has been successfully applied to study the mesophase behavior for a variety of amphiphilic molecule systems [19–34]. Generally speaking, the DPD method simplifies a long series of molecular groups into a few bead-and-spring type particles, and therefore it can simulate the molecular behavior on longer timescales and larger length-scales compared with the traditional molecular dynamics simulation. Groot and Madden [21] were the first who successfully applied DPD on the microphase separation behavior of linear AB diblock copolymers. The phase diagram they constructed in terms of the A composition and the effective A/B segregation parameter is in near quantitative agreement with that predicted by the SCMF theory [35]. Qian et al. [29] applied DPD to construct the phase diagram of cyclic AB diblock copolymers, which they found is very similar to that of linear diblock copolymers. As to examine the phase behavior of miktoarm star copolymers via DPD, which is a quite new research field, only a few related studies have been reported recently. For example, Xu et al. [31] compared the phase behavior of four-arm star copolymers $(AB)_4$ and $(A_2B_2)$, and observed that $(A_2B_2)$ is more likely than $(AB)_4$ to undergo a microphase separation. Qian et al. [32,33] studied the effects of the stiffness of B blocks within $AB_2$ miktoarm star copolymers on the microphase separation.

They found that the increase of the stiffness of the B arms enables the randomly-distributed spheres to pack into an ordered BCC array. Though these past studies have shown that DPD is an appropriate method to examine the mesophase formation of miktoarm star copolymers, a systematic phase behavior has not yet been constructed by DPD. Also, to our knowledge, none of the theoretical studies have been done on analyzing the molecular conformation behavior of miktoarm copolymer chains.

In this paper, we thus aim to employ DPD to simulate the microphase separation behavior and analyze the molecular conformation of three-arm $AB_2$ copolymers. For simplicity, we assume that each component has the same volume per segment (bead). We choose the total number of beads for an $AB_2$ chain to be fixed at $N = N_A + 2N_B = 20$, where $N_A$ and $N_B$ correspond to the number of beads of each arm A and B, respectively, and vary the A composition $f_A = N_A/N$. We first construct the phase diagram in terms of the A composition $f_A$ and the interaction parameter $a_{AB}$, and then quantitatively compare it with the phase diagram obtained by SCMF theory as well as the experimental results. In addition, we analyze the radius of gyration ($R_g$) for each arm A and B, and the total chain $AB_2$, from which the spatial arrangement of each arm within this molecular architecture can be understood.

## 2. DPD simulation method

In the DPD simulation, the time evolution of motion for a set of interacting particles is solved by Newton's equation. For simplicity, we assume that the masses of all particles are equal to 1. The force acting on the $i$-th particle $\vec{f}_i$ contains three parts: a conservative force $\vec{F}^{C}_{ij}$, a dissipative force $\vec{F}^{D}_{ij}$, and a random force $\vec{F}^{R}_{ij}$, i.e.,

$$\vec{f}_i = \sum_{i \neq j} \left( \vec{F}^{C}_{ij} + \vec{F}^{D}_{ij} + \vec{F}^{R}_{ij} \right) \tag{1}$$

where the sum runs over all neighboring particles within a certain cut-off radius $r_c$. As this short-range cut-off counts only local interactions, $r_c$ is usually set to 1 so that all lengths are measured relative to the particle radius.

The conservative force $\vec{F}^{C}_{ij}$ is a soft repulsive force and given by

$$\vec{F}^{C}_{ij} = \begin{cases} a_{ij}\left(1 - \frac{r_{ij}}{r_c}\right)\vec{n}_{ij} & r_{ij} < r_c \\ 0 & r_{ij} \geq r_c \end{cases} \tag{2}$$

where $a_{ij}$ is the repulsive interaction parameter between particles $i$ and $j$, $\vec{r}_{ij} = \vec{r}_i - \vec{r}_j$, $r_{ij} = |\vec{r}_{ij}|$, and $\vec{n}_{ij} = \vec{r}_{ij}/r_{ij}$. The interaction parameter $a_{ij}$ is often related to the Flory–Huggins interaction parameter $\chi_{ij}$ by the following equation [20]:

$$\begin{aligned} a_{ij}(T) &= a_{ii} + 3.497 k_B T \chi_{ij}(T) \quad \text{for } \rho = 3 \\ a_{ij}(T) &= a_{ii} + 1.451 k_B T \chi_{ij}(T) \quad \text{for } \rho = 5 \end{aligned} \tag{3}$$

where $\rho$ is the particle density of the system. The term $a_{ii}$, which corresponds to the interaction parameter between particles of the same type $i$, is determined by matching the water compressibility as [20]

$$a_{ii} = 75 k_B T/\rho \tag{4}$$

The dissipative force $\vec{F}^{D}_{ij}$ is a hydrodynamic drag force and given by

$$F^{D}_{ij} = \begin{cases} -\gamma \omega^{D}(r_{ij})\left(\vec{n}_{ij} \cdot \vec{v}_{ij}\right)\vec{n}_{ij} & r_{ij} < r_c \\ 0 & r_{ij} \geq r_c \end{cases} \tag{5}$$

where $\gamma$ is a friction parameter, $\omega^D$ is a $r$-dependent weight function vanishing for $r \geq r_c$, and $\vec{v}_{ij} = \vec{v}_i - \vec{v}_j$.

The random force $\vec{F}^{R}_{ij}$ corresponds to the thermal noise and has the form of

$$\vec{F}^{R}_{ij} = \begin{cases} \sigma \omega^{R}(r_{ij}) \theta_{ij} \vec{n}_{ij} & r_{ij} < r_c \\ 0 & r_{ij} \geq r_c \end{cases} \tag{6}$$

where $\sigma$ is a parameter, $\omega^R$ is also a weight function, $\theta_{ij}(t)$ is a randomly fluctuating variable. Note that these two forces $\vec{F}^{D}_{ij}$ and $\vec{F}^{R}_{ij}$ also act along the line of centers and conserve linear and angular momentum. There is an independent random function for each pair of particles. Also there is a relation between both constants $\gamma$ and $\sigma$ as follows [20]:

$$\sigma^2 = 2\gamma k_B T \tag{7}$$

In our simulations, $\gamma = 4.5$ and the temperature $k_B T = 1$. As such, $\sigma = 3.0$ according to Eq. (7).

In order for the steady-state solution to the equation of motion to be the Gibbs ensemble and for the fluctuation–dissipation theorem to be satisfied, it has been shown that only one of the two weight functions $\omega^D$ and $\omega^R$ can be chosen arbitrarily [36]:

$$\omega^{D}(r) = \left[\omega^{R}(r)\right]^2 \tag{8}$$

which, in further, is usually taken as

$$\omega^{D}(r) = \left[\omega^{R}(r)\right]^2 = \begin{cases} \left(r_c - r_{ij}\right)^2 & r_{ij} < r_c \\ 0 & r_{ij} \geq r_c \end{cases} \tag{9}$$

Finally, the spring force $\vec{f}^{S}$, which acts between the connected beads in a molecule, has the form of

$$\vec{f}^{S}_{i} = \sum_{j} C \vec{r}_{ij} \tag{10}$$

where $C$ is a harmonic type spring constant for the connecting pairs of beads in a molecule, and is chosen equal to 4 (in terms of $k_B T$) [20].

Note that a modified version of the velocity-Verlet algorithm is used here to solve the Newtonian equation of motion [37]

$$
\begin{aligned}
r_i(t+\Delta t) &= r_i(t) + v_i(t)\Delta t + \tfrac{1}{2} f_i(t)\Delta t^2 \\
\tilde{v}_i(t+\Delta t) &= v_i(t) + \lambda f_i(t)\Delta t \\
f_i(t+\Delta t) &= f_i\left[r_i(t+\Delta t) + \tilde{v}_i(t+\Delta t)\right] \\
v_i(t+\Delta t) &= v_i(t) + \tfrac{1}{2}\Delta t[f_i(t) + f_i(t+\Delta t)]
\end{aligned} \tag{11}
$$

In particular, we choose $\lambda = 0.65$ and $\Delta t = 0.05$ here.

## 3. Results and discussion

In simulating the phase behavior of $AB_2$ miktoarm star copolymers by DPD, the particle density $\rho$ is kept equal to 3, and hence the dimensionless interaction parameter (i.e., in terms of $k_BT$) between equal particles $a_{II}$ in Eq. (4) is set equal to 25 to resemble the Flory interaction parameter $\chi_{II} = 0$; I = A,B. The total number of beads for an $AB_2$ chain is fixed at $N = 20$. We adopt 3-D lattice with at least $15 \times 15 \times 15$ grids to ensure that the side length of the simulation box is significantly larger than the radius of gyration ($R_g$) of $AB_2$ chains. In our simulated systems, the value of $R_g$ is approximately 1.6–2.0 grids. In each pattern, the green and red colors are used to represent A and B, respectively.

Fig. 2 displays the phase diagram of $AB_2$ miktoarm star copolymers simulated by DPD. We also include the phase diagram determined by SCMF theory [8], which is plotted with the black curve in Fig. 2, as a comparison. Similar to linear diblock copolymers, the formation of microstructures is mainly dominated by the composition $f_A$. Fig. 3 illustrates the morphology variation of $AB_2$ with $f_A$ when $a_{AB} = 34$. It is clear that a series of transition from $S_A^{A15}(f_A = 0.2, 0.25) \rightarrow C_A^{HEX}(0.3 \le f_A \le 0.45) \rightarrow$(perforated lamellae of A, $PL_A$) $(f_A = 0.48) \rightarrow$L$(0.5 \le f_A \le 0.7) \rightarrow$(perforated lamellae of B, $PL_B$)$(f_A = 0.75) \rightarrow C_B^{HEX}(f_A = 0.8)$ is observed. Moreover, when the interaction parameter $a_{AB}$ decreases, the ordered $AB_2$ copolymers are expected to become disordered. However, due to the effects of thermal fluctuations, we observe that between the totally disordered and the well-ordered states, the systems tend to form a micelle-like structure, i.e., with chains aggregating as large droplets but no formation of well-ordered structures. Here, we sort it out as the disordered state. Basically these DPD simulated microstructure regimes by varying the composition $f_A$ are in good agreement with the SCMF results except when $f_A$ is larger.

Recall that when $f_A$ is larger, such as $f_A = 0.75$–$0.8$, the SCMF theory predicted a wide region of $C_B^{HEX}$, i.e., the minority B-branch arms form the hexagonally packed cylinders. In our DPD simulations, we find that when the interaction parameter $a_{AB}$ is larger, although the $AB_2$ copolymers can form a stable $C_B^{HEX}$ phase (a typical example when $f_A = 0.8$ and $a_{AB} = 34$ is shown in Fig. 3) eventually, these B-formed cylinders still connect with each other after running a long simulation time. As the interaction parameter $a_{AB}$ decreases, for example when $a_{AB} = 33$ and $f_A$ is still fixed at 0.8, the resulting morphology pattern shown in Fig. 4 clearly demonstrates that these miktoarm star copolymers can no longer form $C_B^{HEX}$ but instead a tube-like phase. A reasonable explanation may be given as follows. When the component with more arms per molecule (i.e., B) is a minority so that these B arms remain on the concave side of the interface, because curving the interface inward toward the B domains causes more lateral crowding of these B multi-arms and thereafter excess stretching in B, the formed microstructures become loose and less ordered. That is, the well-ordered B-formed cylindrical and/or spherical phases are difficult to form and only a tube-like phase is observed. In fact, based on the TEM micrograph similar to the

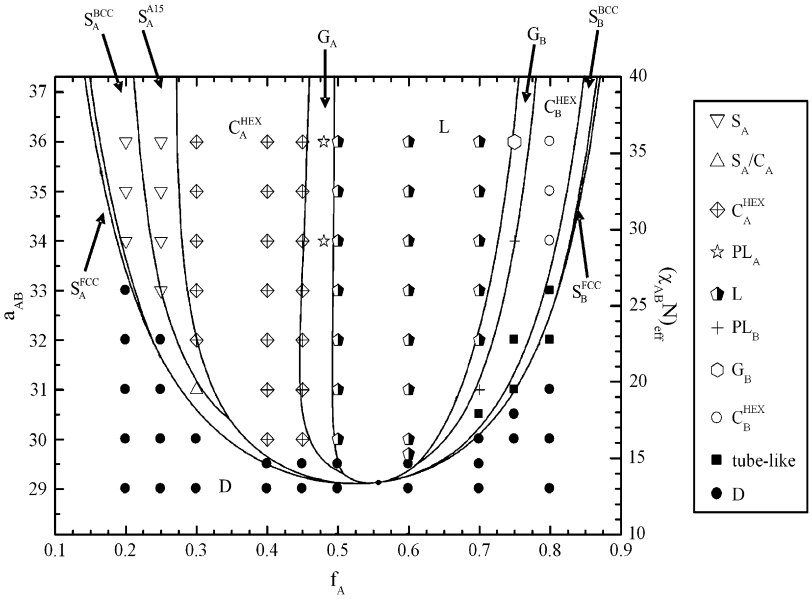


Fig. 2. Phase diagram of $AB_2$ miktoarm star copolymers in terms of the interaction parameter $a_{AB}$ and composition $f_A$. The black solid curves correspond to the phase diagram determined by SCMF theory [8] as a function of $f_A$ and $(\chi_{AB}N)_{eff}$, in which $\chi_{AB}$ is the Flory–Huggins interaction parameter and $N$ is the degree of copolymerization.

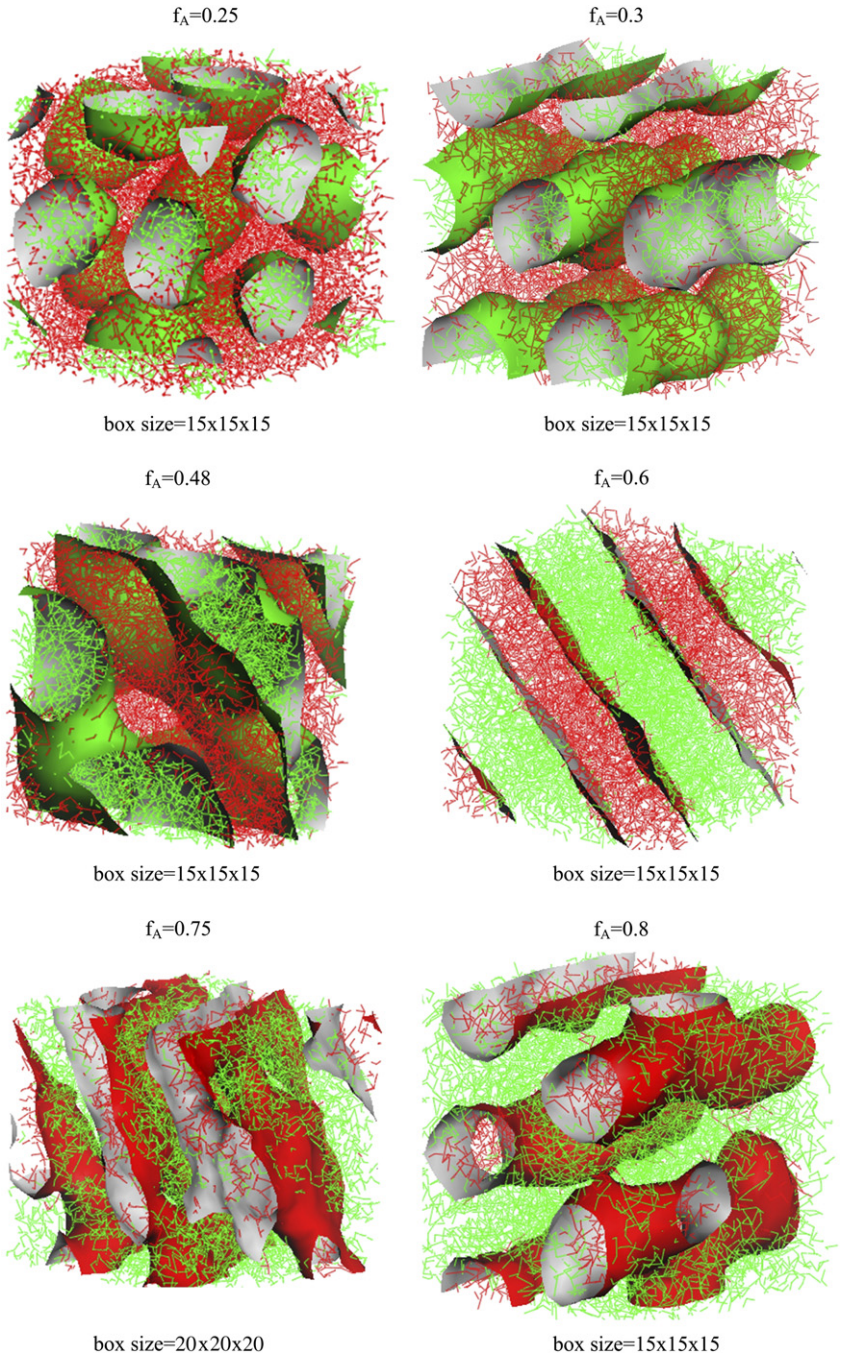


Fig. 3. Morphology variation of $AB_2$ miktoarm star copolymers with $f_A$ at $a_{AB} = 34$. The green and red colors represent A and B, respectively. The green and red surfaces correspond to the isosurfaces of component A and B, respectively. (For interpretation of the references to color in this figure legend, the reader is referred to the web version of this article.)

2-D pattern in Fig. 4, Pochan et al. [11] reported similar results in PS–$PI_2$ miktoarm star copolymers that when the composition of PS, $f_{PS}$, is 0.81, the system is not ordered into a specific lattice but is microphase separated into worm-like micelles, as observed in DPD.

Next, we would like to address whether the above-simulated patterns via DPD are dependent of the finite size of the simulation box, as have been reported in other theoretical studies [38–40]. In order to manifest this, we examine each microstructure in different sizes of the simulation box $L^3$ with $L \geq 10$. When the systems tend to form the spheres as SCMF theory predicted, the packing array of these spheres is strongly dependent of the size of the simulation box even though the box size is much larger than the radius of gyration of $AB_2$ molecules. For example, in Fig. 5(a)–(c) we present the patterns for $AB_2$ with $f_A = 0.25$ and $a_{AB} = 35$, simulated in a box of $12^3$, $15^3$, and $19^3$, respectively. It is clear that the spherical micelles with the radius approximately equal to 3.1 grids are formed in the box of $12^3$, $15^3$, and $19^3$, but they pack into a FCC, A15, and BCC lattice, respectively.

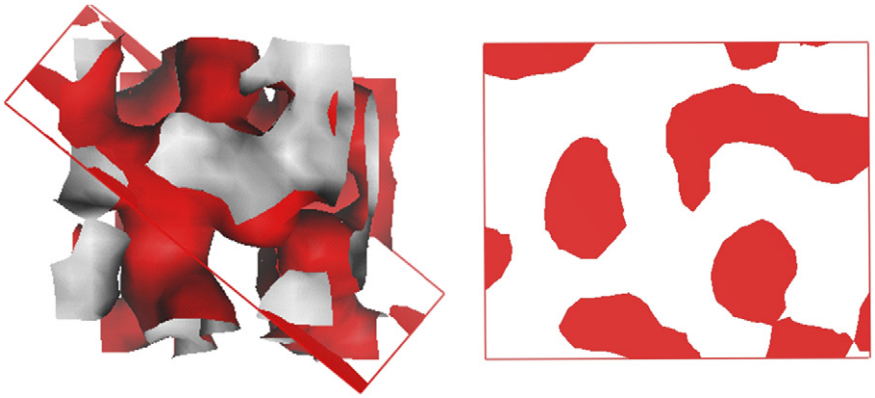

Fig. 4. Morphology pattern and projection of $AB_2$ miktoarm star copolymers with $f_A = 0.8$ and $a_{AB} = 33$.

With a further inspection of Fig. 5(a)–(c), the number of the effective spheres formed in each simulation box is equal to 4, 8, and 16, which simply corresponds to the number of effective spheres in a FCC, A15, and BCC lattice multiplied by 8. These results are not surprising since they are merely the best comprise in the box size, in which the number of formed spheres have to fit the number of spheres required for a specific kind of packing. In order to determine the most stable spherical packing order, one has to keep enlarging the simulation box size till the free energy minimum has been reached. Indeed, though this finite size effect may also occur in other microstructures, such as L and $C^{HEX}$, we observe that when the simulation box size is at least 8–10 times larger than the radius of gyration of molecules (for example, the box size of $L = 15$ is large enough for the molecules with $R_g$ approximately equal to 1.6–2.0 grids here), these ordered L and $C^{HEX}$ regimes are no longer affected by the simulation box. Similar results with respect to the finite size effects have also been observed by Groot and Madden [21].

In order to quantitatively compare the phase diagram determined from both DPD and SCMF theories, we first use Eq. (3) to transform the interaction parameter in the DPD simulations, $a_{AB}$, into the Flory–Huggins interaction parameter in the SCMF theory, $\chi_{AB}$. As the copolymer chains in our simulations are very short ($N = 20$), due to the significant fluctuation effects which stabilize the disordered state, the expected values of $\chi_{AB}N$ at the ODT are larger than those for infinite chains, i.e., $(\chi_{AB}N)_{eff}$, predicted by SCMF theory. Therefore, we have to convert $\chi_{AB}N$ for a finite chain length into $(\chi_{AB}N)_{eff}$ for an infinite chain length. As far as we know, this conversion has not been derived theoretically for $AB_2$ miktoarm star copolymers. We thus simulate the phase behavior for a series of $N$ varying from 10 to 40 at a fixed composition value of $f_A = 0.6$, and analyze the variation of $(\chi_{AB}N)_{ODT}$ with $N$ in Fig. 6. The value of $(\chi_{AB}N)_{ODT}$ for a specific $N$ is determined by averaging the lowest $\chi_{AB}N$ for an ordered state and the highest one for a disordered state, which are designated with error bars in Fig. 6. The log–log plot of $(\chi_{AB}N)_{ODT}/(\chi_{AB}N)_{ODT,eff} - 1$ and $N$, as shown in Fig. 6, reveals a straight line. This manifests the fact that in $AB_2$ miktoarm star copolymers, the decrease of the effective segregation parameter caused by fluctuations for a finite chain $N$ obeys the equation $(\chi_{AB}N)_{eff} = (\chi_{AB}N)/(1 + \alpha N^{\beta})$. From Fig. 6, we obtain the value of $\alpha = 3.2$ and $\beta = -0.43$. We then apply this equation to convert $\chi_{AB}N$ into $(\chi_{AB}N)_{eff}$, and compare our simulated phase diagram with that determined by SCMF theory in Fig. 2. We observe that both phase diagrams are in quantitatively good agreement. Recall that in linear AB diblock copolymers the corresponding ODT value of $\chi_{AB}N$ for a finite chain has been derived by including the fluctuation effects [18], and applied to quantitatively match the phase diagrams between the DPD simulation and SCMF theory [19],

$$(\chi_{AB}N)_{eff} = \frac{\chi_{AB}N}{1 + 3.9N^{\frac{2}{3}-2\nu}} = \frac{\chi_{AB}N}{1 + 3.9N^{-0.51}} \tag{12}$$

where $\nu$ is the swelling exponent for a copolymer chain with $R_g \sim N^{\nu}$. For short polymer chains, they become swollen and $\nu = 0.588$. The fact that both conversion equations are quite similar reveals that the thermal fluctuation effects on the correction for the ODT for a finite chain length are almost consistent in AB linear copolymers and $AB_2$ miktoarm star copolymers.

In order to analyze the molecular conformation behavior of $AB_2$ miktoarm star copolymers, we calculate the radius of gyration, $R_g$, for a chain, which is given as follows:

$$R_g = \left\langle R_g^2 \right\rangle^{\frac{1}{2}} = \left\langle \frac{1}{N}\sum_{i=1}^{N} |\vec{r}_i - \vec{r}_{cm}|^2 \right\rangle^{\frac{1}{2}} \tag{13}$$

where $\vec{r}_i$ and $\vec{r}_{cm}$ are the position vector of the $i$-th bead and center of mass, respectively. Moreover, we also calculate the radius of gyration for each A and B arm by the following equations,

$$R_{g,A} = \left\langle R_{g,A}^2 \right\rangle^{\frac{1}{2}} = \left\langle \frac{1}{N_A}\sum_{i=1}^{N_A} |\vec{r}_{i,A} - \vec{r}_{cm,A}|^2 \right\rangle^{\frac{1}{2}} \tag{14a}$$

$$R_{g,B} = \left\langle R_{g,B}^2 \right\rangle^{\frac{1}{2}} = \left\langle \frac{1}{N_B}\sum_{i=1}^{N_B} |\vec{r}_{i,B} - \vec{r}_{cm,B}|^2 \right\rangle^{\frac{1}{2}} \tag{14b}$$

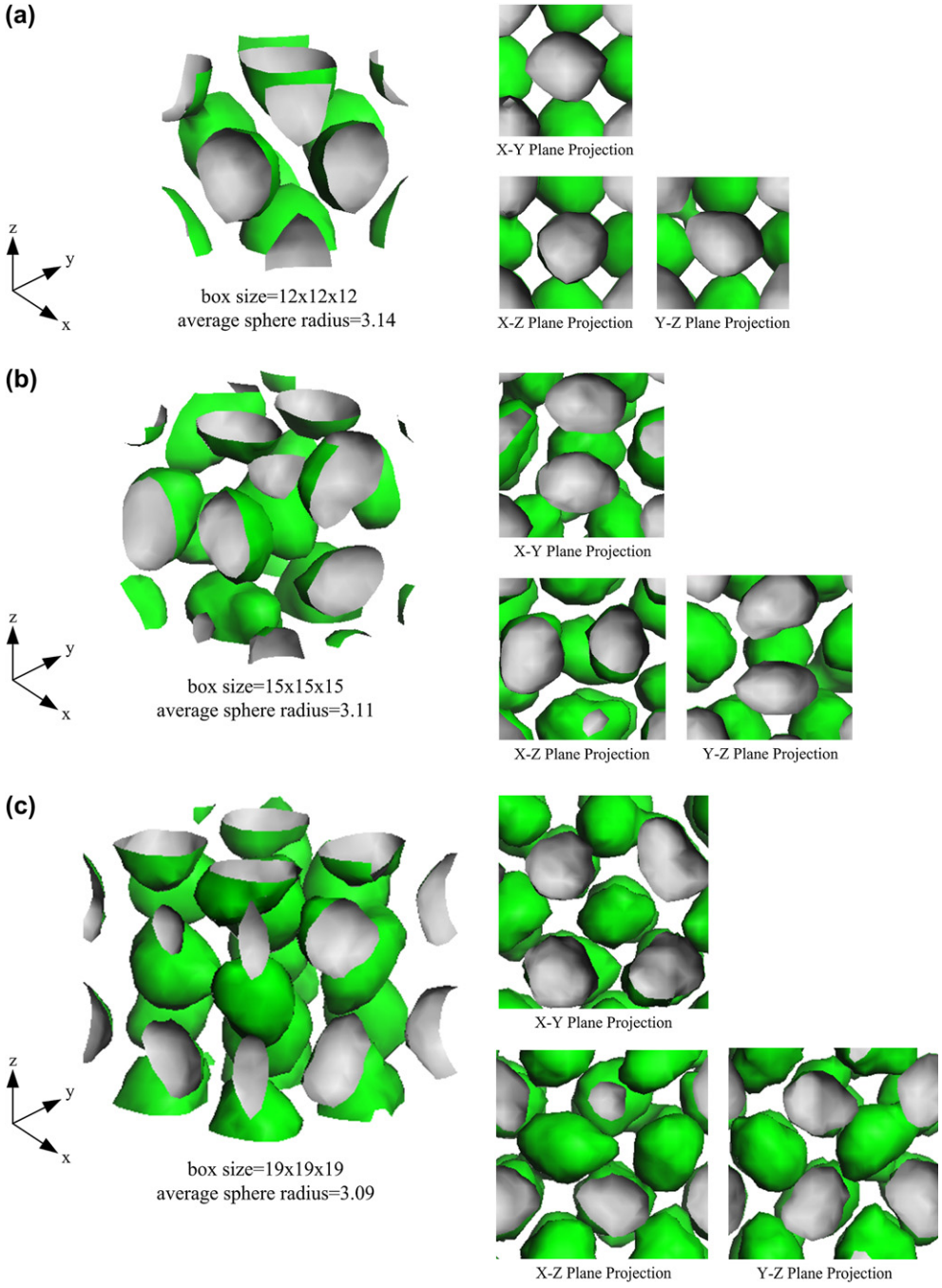


Fig. 5. Morphology patterns of $AB_2$ miktoarm star copolymers with $f_A = 0.25$ and $a_{AB} = 35$, simulated in a box of (a) $12 \times 12 \times 12$, (b) $15 \times 15 \times 15$, and (c) $19 \times 19 \times 19$, respectively. The green surface corresponds to the isosurface of component A. (For interpretation of the references to color in this figure legend, the reader is referred to the web version of this article.)

Fig. 7 shows the variation in $R_g$, $R_{g,A}$, and $R_{g,B}$ with the interaction parameter $a_{AB}$ when $f_A = 0.6$, in which the vertical error bars provide the dispersion of the radius of gyration, expressed as one standard deviation within around $\pm 10\%$. It is clear that when $a_{AB} < 29.5$, which corresponds to the disordered regime, $R_g$ remains approximately at 1.6 grids. As the system enters the ordered regime ($a_{AB} > 29.5$), $R_g$ shows an increasing behavior with $a_{AB}$, and then reaches a constant value of 2.0 grids when $a_{AB} \geq 50$. This significantly increasing trend of $R_g$ near the ODT as $a_{AB}$ increases may be attributed to the increasing stretching degree of each A and B arm, which results in the increase of $R_{g,A}$ and $R_{g,B}$, an/or the mutual expelling degree between A and B arms. However, as can be seen in Fig. 7, $R_{g,A}$ and $R_{g,B}$ barely vary with the interaction parameter $a_{AB}$ even when the system transforms from the disordered into the ordered state. Therefore, the spatial arrangement of each arm becomes a key factor to affect $R_g$ for the whole chain. In order to manifest this, calculating the angles between A/B arms and B/B arms for one $AB_2$ molecule defined as $\theta_{AB}$ and $\theta_{BB}$, respectively, seems to be a straightforward approach.

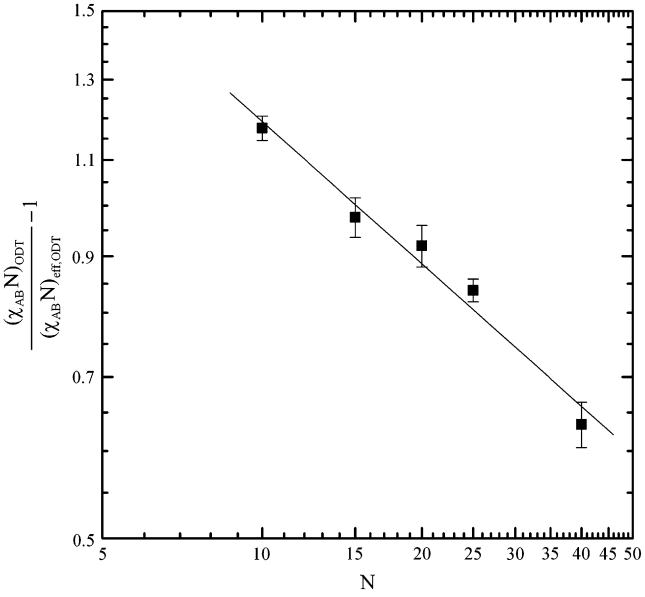


Fig. 6. Log–log plot of $(\chi_{AB}N)_{ODT}/(\chi_{AB}N)_{ODT,eff}-1$ versus $N$ for $AB_2$ miktoarm star copolymers at $f_A=0.6$.

Here the stretching direction for the I-th arm from the branch-point is approximated as the direction of vector of $\overrightarrow{r}_{cm,I}-\overrightarrow{r}_o$, where $\overrightarrow{r}_o$ is the position vector of the branch-point of $AB_2$ molecule. The angle between I-th and J-th arms, $\theta_{IJ}$, can thus easily be calculated through the dot product of $\overrightarrow{r}_{cm,I}-\overrightarrow{r}_o$ and $\overrightarrow{r}_{cm,J}-\overrightarrow{r}_o$. Since the two B arms are symmetric, the angles between A and the two B arms are almost the same, and therefore only one $\theta_{AB}$ is presented. Fig. 8 shows the distribution of $\theta_{BB}$ and $\theta_{AB}$ for $AB_2$ with $f_A=0.6$ at various values of the interaction parameter $a_{AB}$. It can be seen that

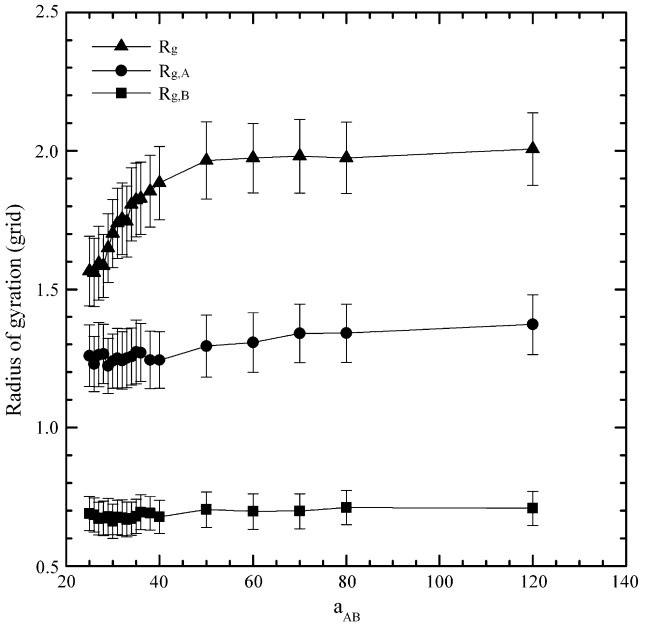


Fig. 7. Plot of radius of gyration ($R_g$, $R_{g,A}$, $R_{g,B}$) for $AB_2$ miktoarm star copolymers with $f_A=0.6$ versus the interaction parameter $a_{AB}$.

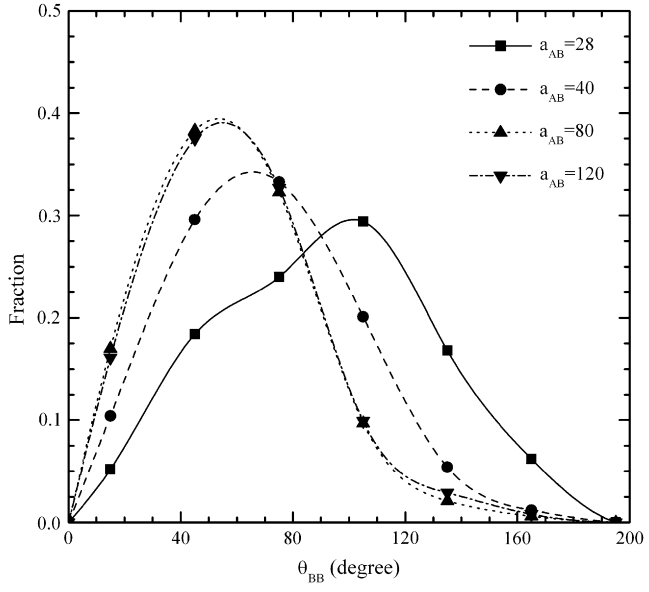


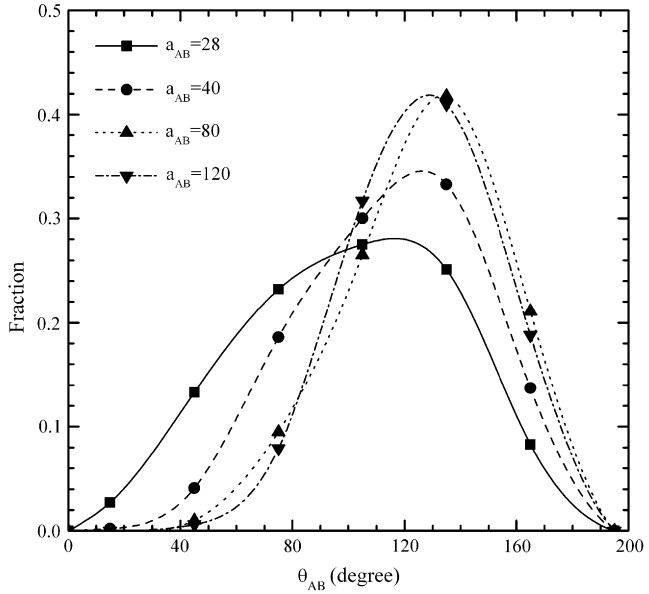


Fig. 8. Distribution of $\theta_{BB}$ and $\theta_{AB}$ for $AB_2$ miktoarm star copolymers with $f_A=0.6$ at various values of the interaction parameter $a_{AB}$.

when $a_{AB}=28$, these disordered $AB_2$ copolymer chains can distribute relatively more freely in the space, and therefore, both $\theta_{BB}$ and $\theta_{AB}$ demonstrate a broader distribution. As $a_{AB}$ increases, each distribution profile becomes narrower, and the distribution of $\theta_{BB}$ moves toward smaller angles while the distribution of $\theta_{AB}$ shifts to larger angles. This manifests the fact that when the system enters into an ordered state, in order to reduce the contacts between A and B, the A and B arms tend to separate from each other, and the two B arms are squeezed onto the same side.

Basically, the above results of the molecular conformation behavior by varying the effects of the interaction parameter $a_{AB}$ for $f_A=0.6$ also hold true qualitatively for the systems with other compositions. Next, we discuss how the molecular conformation varies with $f_A$ at the same $a_{AB}$. Fig. 9 presents

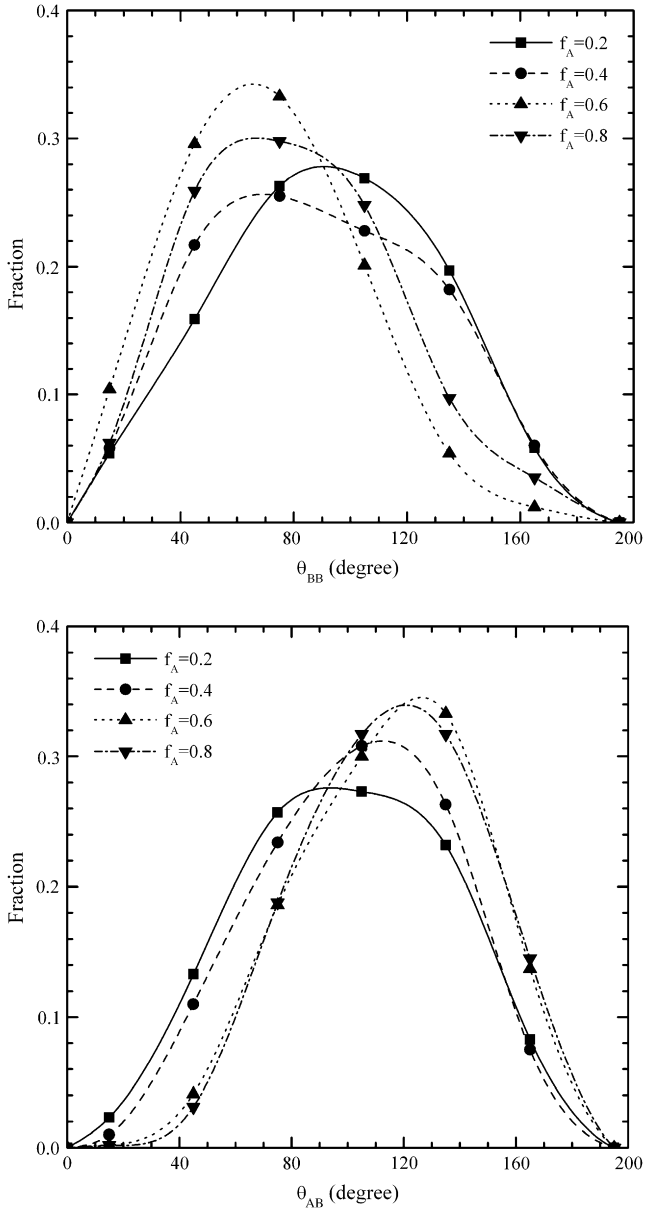


Fig. 9. Distribution of $\theta_{BB}$ and $\theta_{AB}$ for $AB_2$ miktoarm star copolymers with $a_{AB} = 40$ at various values of the composition $f_A$.

the distribution of $\theta_{BB}$ and $\theta_{AB}$ at various values of $f_A$ when $a_{AB} = 40$. We observe that when $f_A$ increases to about 0.6 so that the molecules become more symmetric, due to the increase of the mutual repelling degree between A and B, the peak of $\theta_{AB}$ increases and the peak of $\theta_{BB}$ decreases. As $f_A$ continues to increase further, since the molecules become more asymmetric and thereafter the mutual A/B segregation effects reduce, the peak of $\theta_{AB}$ and $\theta_{BB}$ shows a decreasing and increasing trend, respectively.

## 4. Conclusions

We employ dissipative particle dynamics (DPD) to examine the phase behavior and molecular conformation behavior of $AB_2$ miktoarm star copolymers by varying the composition and the interaction parameter. Similar to linear AB diblock copolymers, our simulated phase diagram reveals that the formation of possible ordered structures, such as lamellae, gyroid, perforated lamellae, hexagonally packed cylinders, and ordered spheres, is mainly dominated by the composition. These DPD simulated microstructure regimes by varying the composition are typically in good agreement with those predicted by self-consistent mean-field (SCMF) theory. Through a mapping of the interaction parameter for a finite chain length, we find that the phase diagram via DPD is in near quantitative agreement with that predicted by SCMF theory. However, when the A composition is large such that the SCMF theory predicts a hexagonally packed B-formed cylindrical phase, our DPD results demonstrate that these $AB_2$ chains are not able to form the well-ordered structure as easily as the SCMF theory has predicted, but instead only a tube-like phase. This is because when the B multi-arms remain on the concave side of the interface, curving the interface inward toward the B domains causes more lateral crowding and thereafter excess stretching in B. Hence, the formed microstructures become less ordered. Indeed, these DPD results are more consistent with the experimental results, as the SCMF theory ignores the possibility of aggregates without specific packing order.

In analyzing the molecular conformation behavior of $AB_2$ molecules, we observe that the radius of gyration ($R_g$) for the whole $AB_2$ chain significantly increases with the interaction parameter while the $R_g$ values of each A and B arm remain relatively unchanged. Furthermore, the angle between A and B arms shows an increasing trend while the angle between B and B arms shows a decreasing behavior with the interaction parameter. These results manifest the fact that in order to reduce the contacts between A and B, the A and B arms tend to separate from each other, and the two B arms are squeezed onto the same side. Similar variation behavior has also been observed when the composition of A and B becomes more symmetric.

## Acknowledgements

This work was supported by the National Science Council of the Republic of China through grant NSC 95-2221-E-002-155.

## References

[1] Hadjichristidis N, Pispas S, Floudas G. Block copolymers: synthetic strategies, physical properties, and applications. New Jersey: Wiley; 2003.
[2] Edens MW, Whitmarsh RH. In: Hamley IW, editor. Developments in block copolymer science and technology. New York: Wiley; 2004.
[3] Hamley IW. The physics of block copolymers. Oxford: Oxford University Press; 1998.
[4] Lodge TP. Macro Chem Phys 2003;204:265.
[5] Olvera de la Cruz M, Sanchez IC. Macromolecules 1986;19:2501.
[6] Milner ST. Macromolecules 1994;27:2333.
[7] Olmsted PD, Milner ST. Macromolecules 1998;31:4011.
[8] Grason GM, Kamien RD. Macromolecules 2004;37:7371.
[9] Hudson SD, Jung HT, Percec V, Cho WD, Johansson G, Ungar G, et al. Science 1997;278:449.
[10] Grason GM, DiDonna BA, Kamien RD. Phy Rev Lett 2003;91:583041.

[11] Pochan DJ, Gido SP, Pispas S, Mays JW, Ryan AJ, Fairclough JPA, et al. Macromolecules 1996;29:5091.
[12] Floudas G, Pispas S, Hadjichristidis N, Pakula T, Erukhimovich I. Macromolecules 1996;29:4142.
[13] Tselikas Y, Iatrou H, Hadjichristidis N, Liang KS, Mohanty K, Lohse DJ. J Chem Phys 1996;105:2456.
[14] Lee C, Gido P, Pitsikalis M, Mays JW, Tan NB, Trevino SF, et al. Macromolecules 1997;30:3732.
[15] Hadjichristidis N. J Polym Sci A Polym Chem 1999;37:857.
[16] Yang L, Hong S, Gido SP, Velis G, Hadjichristidis N. Macromolecules 2001;34:9069.
[17] Mavroudis A, Avgeropoulos A, Hadjichristidis N, Thomas EL, Lohse DJ. Chem Mater 2003;15:1976.
[18] Fredrickson GH, Helfand E. J Chem Phys 1987;87:697.
[19] Groot RD, Madden TJ, Tildesley DJ. J Chem Phys 1999;110:9739.
[20] Groot RD, Warren PB. J Chem Phys 1997;107:4423.
[21] Groot RD, Madden TJ. J Chem Phys 1998;108:8713.
[22] Groot RD. Langmuir 2000;16:7493.
[23] Yamamoto S, Maruyama Y, Hyodo S. J Chem Phys 2002;116:5842.
[24] Ryjkina E, Kuhn H, Rehage H, Muller F, Peggau J. Angew Chem Int Ed 2002;41:983.
[25] Rekvig L, Kranenburg M, Vreede J, Hafskjold B, Smit B. Langmuir 2003;19:8195.
[26] Schulz SG, Kuhn H, Schmid G, Mund C, Venzmer J. Colloid Polym Sci 2004;283:284.
[27] Groot RD. Lect Notes Phys 2004;640:5.
[28] Kuo MY, Yang HC, Hua CY, Chen CL, Mao SZ, Deng F, et al. Chem Phys Chem 2004;5:575.
[29] Qian HJ, Lu ZY, Chen LJ, Li ZS, Sun CC. Macromolecules 2005; 38:1395.
[30] Cao X, Xu G, Li Y, Zhang Z. J Phys Chem A 2005;109:10418.
[31] Xu Y, Feng J, Liu HL, Hu Y. J East China Univ Sci Tech 2006; 32:133.
[32] Qian HJ, Chen LJ, Lu ZY, Li ZS, Sun CC. J Chem Phys 2006;124: 14903.
[33] Qian HJ, Chen LJ, Lu ZY, Li ZS, Sun CC. Europhys Lett 2006; 74:466.
[34] Huang CI, Hsueh HY, Lan YK, Lin YC. Macromol Theory Simul 2007;16:77.
[35] Matsen MW, Bates FS. Macromolecules 1996;29:1091.
[36] Espanol P, Warren PB. Europhys Lett 1995;30:191.
[37] Allen MP, Tildesley DJ. Computer simulation of liquids. Oxford: Clarendon; 1987.
[38] Micka U, Binder K. Macromol Theory Simul 1995;4:419.
[39] Bahbot-Raviv Y, Wang ZG. Phys Rev Lett 2000;85:3428.
[40] Wang Q, Nealey PF, de Pablo JJ. Macromolecules 2001;34:3458.